Soft Matter

Accepted Manuscript

This article can be cited before page numbers have been issued, to do this please use: A. Moncho Jorda and I. Adroher-Benítez, *Soft Matter*, 2014, DOI: 10.1039/C4SM00243A.

ROYAL SOCIETY OF CHEMISTRY

www.rsc.org/softmatter

ARTICLE TYPE www. rsc.org/xxxxxx | XXXXXXXX

Ion permeation inside microgel particles induced by specific interactions: from charge inversion to overcharging

View Article Online
DOI: 10.1039/C4SM00243A

A. Moncho-Jordá,*[a] and I. Adroher-Benítez,[a]

Received Xth XXXXXXXXXX 20XX, Accepted Xth XXXXXXXXX 20XX
First published on the web Xth XXXXXXXXXX 200X
DOI: 10.1039/b000000x

In this work we have performed a theoretical study of the system formed by ionic microgels in the presence of monovalent salt with the help of the Ornstein-Zernike integral equations within the Hypernetted-Chain (HNC) approximation. We focus in particular on analysing the role that the short-range specific interactions between the polymer fibres of the microgel and the incoming ions have on the equilibrium ion distribution inside and outside the microgel. For this purpose, a theoretical model based on the equilibrium partitioning effect is developed to determine the interaction between the microgel particle and a single ion. The results indicate that when counterions are specifically attracted to the polymer fibres of the microgel, an enhanced counterion accumulation occurs that induces the charge inversion of the microgel and a strong increase of the microgel net charge (or *overcharging*). For the case of coions, the specific attraction is also able to provoke the coion adsorption even though they are electrostatically repelled, and so increasing the microgel charge (*true overcharging*). Moreover, we show that the ion adsorption onto the microgel particle is very different in the swollen and shrunken states due to the competition between specific attraction and steric repulsion. In particular, ion adsorption occurs preferentially in the internal core of the particle for swollen states, whereas it is mainly concentrated in the external shell for de-swollen configurations. Finally, we observe the existence of a critical salt concentration, where the net charge of the microgels vanishes; above this inversion point the net charge of the microgels increases again, thus leading to reentrant stability of the microgel suspension.

1 Introduction

Microgels are colloidal particles made up of cross-linked polymer chains dispersed in a solvent. Nowadays they also might be called "nano", since particle size fall within a range of 10–1000 nm[1]. Their most remarkable characteristic is that they are able to swell or to shrink, depending on many external parameters such as pH, temperature, salt concentration or solvent nature[2,3]. The ability to swell reversibly in a thermodynamically good solvent makes microgels very useful for many biotechnological applications[4,5]. Recently, these particles have shown very advantageous properties for designing smart drug delivery systems responsive to biological stimuli[6,7]. Encapsulation of therapeutic molecules in a microgel particle would protect them from degradation inside the human body, so microgels are being widely investigated for many types of drugs.[8].

For such biotechnological purposes, ionic microgels (formed by a cross-linked network of charged polymers or polyelectrolytes) have shown to be remarkably important, when we are dealing with charged solutes. In this sense, theoretical models have been developed to study the permeation of ions inside the microgel assuming that coions and counterions are exclusively affected by electrostatic interactions[9–14]. However, in addition to the electrostatic interaction, ions are also affected by the existence of excluded volume repulsive forces that arise when they diffuse inside the porous polymer network. This interaction causes the partitioning effect, which makes the electrolyte concentration inside an inert porous medium be smaller than its concentration in the bulk phase[15,16]. In a recent paper, we employed the concepts of equilibrium partitioning to deduce a ion-microgel repulsive steric pair potential which depends on the thickness of the polymer fibres, the size of the ion and the degree of swelling of the microgel particle[17].

But the reader should keep in mind that, in many situations, electrostatic and steric interactions are not the only relevant contributions, as the incoming electrolyte is also able to interact with the polymer network through attractive or repulsive specific forces. This is especially true for this kind of permeable particles, where polymer chains are exposed to the solvent even in internal parts of the particle. Indeed, these interactions are mainly associated to changes in water structure (around the solute and the solvated polymer chain), or to ion adsorption-exclusion effects at interfaces induced by the hydrophobic/hydrophilic nature of the polymer[18–20]. All these phenomena connected to processes and energies of ion

* *Corresponding author. E-mail: moncho@ugr.es*
[a] *Departamento de Física Aplicada, Facultad de Ciencias, Universidad de Granada, Campus Fuentenueva S/N, 18071 Granada, Spain*

solvation are usually known as Hofmeister effects[21]. In particular, ions that enhance water's hydrogen bonded structure are known as kosmotropes, whereas ions that make this structure looser are called chaotropes. The connection between the Hofmeister series and structural rearrangements in the water network induced by ions near interfaces has been evidenced by many authors[22–26]. Although the range of these forces is usually very small (of few water molecule diameters), the strength can be significantly large, giving rise to a noteworthy accumulation/exclusion of ions inside the microgel, which is able to induce important modifications of the net charge of the microgel[27,28]. For instance, the adsorption of anions inside deswollen PNIPAM microgels becomes greatly enhanced when the salt is changed from NaCl to $NaNO_3$, and then to NaSCN (i.e. with the chaotropic character of the anion). In the case of SCN^-, the accumulation is so strong that can induce the charge reversal of cationic microgel particles[21]. Furthermore, the de-swelling process that this particles undergo by salt addition also depends on the Hofmeister nature of the salt. In this sense, there are experimental evidences indicating that kosmotropic ions (such as SO_4^{2-} or F^-) yield a more efficient disruption of the hydrogen-bonded cage responsible for the polymer-hydration, which causes the microgel shrinking at a lower salt concentration[21,28].

In view of that, the main goal of this work is to investigate the role that the short-ranged specific interactions between the polymer fibres of the microgel and the incoming ions have on the ion distribution, the net charge of the particle and the effective microgel-microgel electrostatic interaction. The study is done under different conditions of particle swelling and several specific interactions running from attractive to repulsive potentials. As it will be shown later on, this specific interaction has deep implications on the ionic density profiles and the net charge of the particle. Moreover, it is responsible for an enhanced accumulation or exclusion of counter- or coions that leads to charge inversion and overcharging effects. It should be emphasized that these phenomena are not caused by the electrostatic adsorption of multivalent ions onto a charged surface[29], but instead they are purely driven by these short-range specific forces.

In order to study the effect of the microgel-ion specific interactions, a new analytical model for the steric-specific microgel-ion interaction based on the equilibrium partitioning effect is developed. We hope that this study will represent a useful reference to provide a better understanding of the vast experimental observations obtained with this kind of systems. Calculations are performed solving the Ornstein-Zernike (OZ) integral equations[30,31] within the Hypernetted-Chain HNC approximation. We focus on the limit of infinite dilution of microgel particles, where many-body interactions can be neglected. In this limit, it is known that HNC has some important advantages over other popular integral equations closures such as Percus-Yevick or Rogers-Young. For example it is exact for the Asakura-Oosawa model at all densities[32], and it usually performs quite well for the kind of soft potentials derived in this work, regardless their attractive or repulsive character[33]. Moreover, the net charge and the effective interactions of perfectly permeable microgel particles calculated with the HNC approximation are in excellent agreement with previous theoretical predictions obtained using linear response theory[10,34]. It should be noted that computer simulation also represents a very powerful technique for accurately studying the swelling behaviour, the counterion valence and the ion permeation for a given interaction[35,36]. However, the method employed here is less numerically demanding than computer simulations. It also presents advantages compared to other coarse-grained methods, such as Poisson-Boltzmann theory, since it incorporates the effects arising from the finite size of the ions. Furthermore, OZ integral equations provide a way to perform coarse-graining of the ion degrees of freedom, and to determine unambiguously the effective potential between pairs of microgels in the diluted regime[37,38].

The paper is outlined in the following way. In Section 2 we present the theoretical model of the microgel, describing the mass and charge distribution inside the particle. We also define the concept of partitioning coefficient and describe the ion-ion, microgel-ion, and microgel-microgel bare interactions. The specific polymer-ion bare interaction is highlighted in order to study the ion permeation phenomena. In Section 3 the integral method is briefly explained, while Section 4 depicts the theoretical results for the ionic density profiles around and inside the porous microgel particle, the net charge of the microgel particle, and the microgel-microgel effective pair potential. Finally, we summarize the main conclusions in Section 5.

2 Model

The model system studied here is constituted by spherical microgel particles immersed in a monovalent size-symmetric 1:1 electrolyte, with the solvent considered as a uniform dielectric background. Therefore, the system is as a ternary mixture in equilibrium of N_m microgels, N_+ counterions and N_- coions, with bare charges given by $-Ze$, $+e$ and $-e$, respectively (e is the elementary charge), where $N_+ = N_- + ZN_m$ in order to satisfy the electro-neutrality condition. Before describing the particle-particle bare interactions, we need a model for the polymer mass and charge distribution inside the microgel network, and for the internal structure of the polymer fibres. These points are addressed in the following subsections.

View Article Online
DOI: 10.1039/C4SM00243A

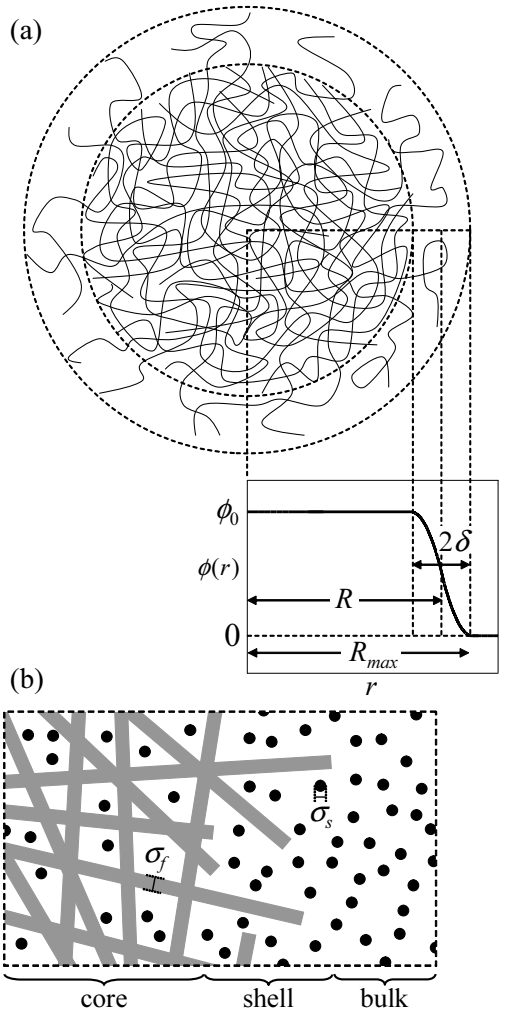

Fig. 1 (a) Schematic view of the internal structure of a core-shell microgel particle. The plot shows the polymer packing fraction as a function of the distance from the particle center. R and 2δ are the half-width radius and the shell size, respectively. Analogously, the external radius of the particle is $R_{max} = R + \delta$. (b) This figure illustrates the model used in this work for the polymer fibres, represented by randomly oriented cylinders of diameter $\sigma_f = 2R_f$, and the ions, with diameter $\sigma_s = 2R_s$.

2.1 Mass and charge distribution of ionic microgels

Microgel particles are not homogeneous spheres, as the internal region has usually a larger polymer density than the external one. This is caused by the faster consumption of cross-linker molecules than of monomer during the initial stages of the synthesis[39,40]. Therefore, microgels are in general particles with a core-shell structure, having a more concentrated, highly cross-linked core, surrounded by a fuzzy corona where the polymer density decays gradually to zero[41–43]. In this work, the radial polymer packing fraction is assumed to be described with a symmetric form based on a parabolic shape[43]

$$\phi(r) = \phi_0 \begin{cases} 1 & r \le R-\delta \\ 1-\frac{1}{2}\left(\frac{r-R+\delta}{\delta}\right)^2 & R-\delta \le r < R \\ \frac{1}{2}\left(\frac{R-r+\delta}{\delta}\right)^2 & R \le r < R+\delta \\ 0 & r > R+\delta \end{cases} \quad (1)$$

where ϕ_0 is the polymer packing fraction at the particle core, R is the particle half-width radius, 2δ is the thickness of the interface (shell), and $R_{max} = R + \delta$ is the external radius of the microgel particle (see Fig 1(a)). This model has been proved to give a fair description of the microgel mass distribution in the swollen and de-swollen states, and in any intermediate swelling conformation[44]. For a swollen microgel, the packing fraction is usually low ($\phi_0 \lesssim 0.1$), and the shell extension is relatively large, giving rise to a smooth interface. In the collapsed configuration, both the core and shell size decrease, leading to denser particles ($\phi_0 \gtrsim 0.5$) with a sharp interface ($\delta << R$).

Since charged co-monomers are distributed in the polymer matrix, most of them will be located inside the core, with a lower density that gradually decrease with the distance to the particle center in the shell[45,46]. In this work the charge density is assumed to follow the same distribution than the radial density profile,

$$\rho_e(r) = \rho_{e0}\frac{\phi(r)}{\phi_0}, \quad (2)$$

where ρ_{e0} is the density charge in the core. This is a quite reasonable approximation, considering that the microgel network is generated during the synthesis process by cross-linking of ionic polymer chains. The microgel bare charge can be obtained from integration of the charge distribution, leading to $Z = (2\pi\rho_{e0}/3e)(2R^3 + R\delta^2)$[9]. In any case, the model and the method that will be presented below can be easily extended to other charge distributions.

2.2 Partitioning coefficient

It is a well–established experimental evidence that the concentration of a neutral solute inside an inert porous or fibrous medium is smaller than its concentration in the bulk

phase[15,16]. In other words, the solute is affected by an excluded volume repulsive force that partially hinders the diffusion of solute inside the porous medium. This phenomenon is known as partitioning effect, and appears in many separation process in the presence of membranes or gels[47,48].

We consider the system formed by a bulk suspension of uncharged spheres (solute) with radius R_s in equilibrium with a homogeneous fibrous network. Both the porous medium and the bulk phase are filled by a common solvent. It is well established that within these conditions, a concentration difference of solute arises between the pore and bulk phases, causing the partitioning of the solute[15,16]. The difference becomes more pronounced when the size of the solute is of the same order of magnitude than the pore size. The partitioning coefficient is defined as the ratio between the number density of spheres inside the fibrous network and the number density in the bulk.

$$K = \frac{\rho_s}{\rho_{0s}}. \tag{3}$$

In general, K depends on the geometry of the porous structure (cylindrical, spherical, thin slits,...), the solute-solute and solute-pore interactions (hard core, electrostatic,...) and also on the number density of solute in the bulk[49–52]. The internal structure of a fibrous material or cross-linked polymeric gel is usually modelled as a randomly oriented assembly of infinitely long and mutually interpenetrable hard cylindrical fibres of radius R_f. According to this model, the probability density of finding the sphere at a distance r from the closest fibre for dilute solutions is given by[15,53]

$$P(r) = \frac{2\phi' r}{{R_f}^2} e^{-\phi'(r/R_f)^2} e^{-\beta V_{sf}(r)}, \tag{4}$$

where $\beta = 1/(k_B T)$, $V_{sf}(r)$ is the solute-fibre interaction potential. ϕ' represents the volume fraction of polymer fibres without taking into account the overlap between them. However, inside a microgel particle, fibres are actually overlapping in the cross-linker nodes, so the real volume fraction (ϕ) is always smaller[15]. For the case of straight cylindrical fibres randomly and isotropically distributed inside a uniform microgel, the relation between ϕ' and ϕ is given by $\phi' = -\ln(1-\phi)$. Hence,

$$P(r) = -\frac{2\ln(1-\phi) r}{{R_f}^2} e^{\ln(1-\phi)(r/R_f)^2} e^{-\beta V_{sf}(r)}. \tag{5}$$

The partitioning coefficient for a dilute solution is obtained from

$$K = \int_0^\infty P(r) dr. \tag{6}$$

In the pioneering paper by Ogston[53], he only considered the steric exclusion created by the fibre matrix. Thus,

$$V_{sf}(r) = \begin{cases} \infty & r \le R_s + R_f \\ 0 & r > R_s + R_f \end{cases} \tag{7}$$

which leads to

$$K = e^{\ln(1-\phi)(1+R_s/R_f)^2}. \tag{8}$$

This model has been found to yield very good predictions for the solute permeation inside agarose gels, where the steric repulsion is the dominant interaction[54]. However, in the present work we are mainly interested in including a short-range specific interaction between the fibre and the approaching solute. The physical origin of this interaction may be very different depending on the size and nature of the solute and the fibre. For instance, it is attractive between a hydrophobic polymer fibre and a chaotropic solute, and repulsive when dealing within a hydrophilic fibre and a kosmotropic solute[21]. Here, we do not really need to have the exact details of such specific interaction, as the more relevant feature is its short-range character. In order to deduce an analytical expression for K, we will assume that the fibre-solute interaction is represented by a square barrier (or square well) of width Δ

$$V_{sf}(r) = \begin{cases} \infty & r \le R_s + R_f \\ V_0 & R_s + R_f < r \le R_s + R_f + \Delta \\ 0 & r > R_s + R_f + \Delta \end{cases} \tag{9}$$

The integration of the probability density according to Eq. 6 yields the following partition coefficient

$$\begin{aligned} K &= (1 - e^{-\beta V_0}) e^{\ln(1-\phi)\left(1+\frac{R_s+\Delta}{R_f}\right)^2} \\ &+ e^{-\beta V_0} e^{\ln(1-\phi)\left(1+\frac{R_s}{R_f}\right)^2} \end{aligned} \tag{10}$$

As observed, this expression enclose both, the steric and the specific contributions. In the limit $V_0 \to 0$ or $\Delta \to 0$, we recover the Ogston model for inert fibrous cross-linked networks (see Eq. 8).

Although the present model has been originally developed for homogeneous fibrous polymer networks, it may be easily extended to our heterogeneous core-shell cross-linked microgel particles by including the dependence of the volume fraction on the distance to the particle centre, $\phi(r)$. A schematic illustration of the internal structure of a core-shell microgel particle is shown in Fig. 1(b). By this simple procedure we finally obtain a partitioning coefficient $K(r)$ that continuously varies from the value in the core K_{core} to 1 when $r = R_{max}$.

Fig. 2 shows the value of K obtained from Eq. 10 as a function of the packing fraction for several values of V_0, and assuming that $R_f = 0.4$ nm and $R_s = \Delta = 0.175$ nm. As it may be observed, for repulsive specific interactions ($V_0 > 0$) $K(\phi)$ decreases from 1 at $\phi = 0$ (no polymer network) to 0 for $\phi = 1$ (no free space for the incoming solute). On the contrary, it is interesting to note that this monotonic behaviour breaks down as soon as the specific interaction becomes attractive ($V_0 < 0$). Then, there is an interplay between the attractive counterpart

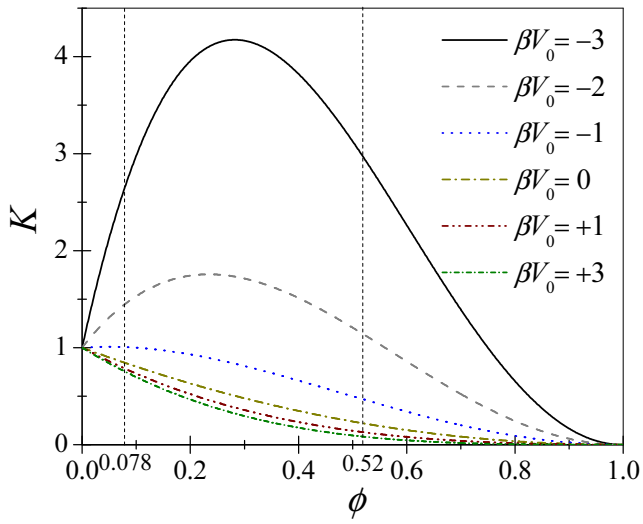

Fig. 2 Partitioning coefficient obtained from Eq. 10 versus the volume fraction of the cross-linked polymer network. Curves correspond To different strengths of the specific interaction, from attraction ($V_0 < 0$) to repulsion ($V_0 > 0$). The plots are for $R_f = 0.4$ nm, and $R_s = \Delta = 0.175$ nm.

of the solute-fibre interaction and the repulsive steric exclusion, both of them growing with ϕ. For low enough ϕ the attraction is always the dominant term, whereas the steric repulsion becomes the most important contribution for $\phi \to 1$. As a result of this competition, a maximum of the partitioning coefficient is found for an intermediate volume fraction, which grows with the strength of the attraction.

It should be emphasized that Eq. 10 only considers the interaction between the solute and its nearest fibre [15]. Therefore, this approximation is only realistic when the range of the specific interaction (namely $R_s + \Delta$) is smaller than the interfibre spacing inside the cross-linked polymer network. This means that the model cannot be applied when the polymer volume fraction is so large that any incoming solute is simultaneously affected by the presence of two or more fibres. In order to find out when Eq. 10 holds, we assume here that the polymer fibres are arranged in a cubic lattice of length L, with the cross-linker monomers located at the vertexes, and connecting six chains (see Fig. 3). Although the real internal structure and the cross-linker connectivity may be different, we expect this approximation to be good enough to estimate an upper bound for the interaction range. According to this model, the volume fraction is given by the ratio between the volume occupied by the polymer inside a single cubic cell, V_{pol}, and the volume of the unit cell

$$\phi \approx \frac{V_{pol}}{L^3} = 1 - \left(1 - 2\frac{R_f}{L}\right)^3 - 6\frac{R_f}{L}\left(1 - 2\frac{R_f}{L}\right)^2. \quad (11)$$

The overlap between two interaction regions occurs when $L - 2(R_f + R_s + \Delta) < 0$. Therefore, the condition for the validity of Eq. 10 is

$$\frac{R_s + \Delta}{R_f} < \frac{1}{2R_f/L} - 1. \quad (12)$$

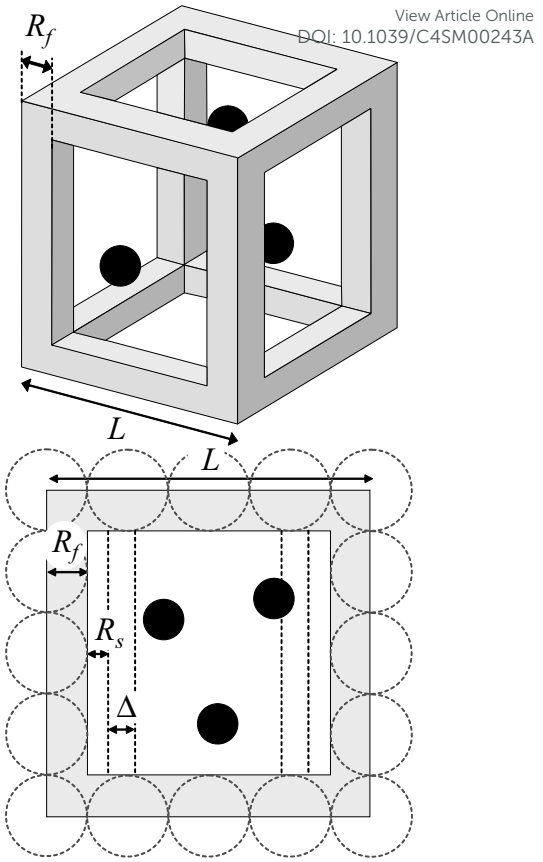

Fig. 3 Simple model for the internal structure of the cross-linked polymer network, where the polymer chains are assumed to be arranged onto a cubic lattice. L is the length of the unit cell, R_f is the fibre radius, R_s the solute radius and Δ is the range of the specific interaction.

In particular, for $R_f = 0.4$ nm and $R_s = \Delta = 0.175$ nm, equations 11 and 12 predict that the model could be applied for polymer volume fractions lower than $\phi = 0.55$.

2.3 Particle interactions

Once the internal charge density of the microgel particles and the partitioning coefficient have been specified, we proceed with the description of the bare interactions between microgel particles, counterions and coions. In this work, the ionic species are modelled as charged hard-core spheres, and so allowing the finite size correlations to be explicitly considered. Therefore, the interaction potential between two ions at dis-

tance r is

$$\beta V_{ij}(r) = \begin{cases} \infty & r \leq R_i + R_j \\ z_i z_j L_B / r & r > R_i + R_j \end{cases} \quad (13)$$

where z_i and z_j are the ion valences ($+1$ and -1 for counterions and coions, respectively), $L_B = e^2/(4\pi\varepsilon k_B T)$ is the Bjerrum length (ε is the dielectric permittivity of water and k_B the Boltzmann constant), and $\beta = 1/(k_B T)$. We assume that both counter- an coions have the same radius, given by $R_+ = R_- = 0.36$ nm, which represents an average value for hydrated monovalent ions[55].

The bare interaction between a pair of microgel particles is rather complicated, as it incorporates electrostatic, steric, elastic and London-van der Waals terms that strongly depend on the degree of swelling of the particles, the extension of the shell and, in general, on the internal structure of the polymer network (as the cross-linker density or the degree of connectivity of the cross-linker monomers). All these interactions play a decisive role on determining the phase diagram, the structure and the rheological properties of ionic microgel suspensions, especially for dense systems[1,12,34,56–58]. However, in this work only the electrostatic contribution is actually employed, since as we will show in Section 3, our method does not need the knowledge of the complete microgel-microgel pair potential to obtain the ionic density profiles around the microgel and the electrostatic effective interaction in the limit of very diluted microgel suspensions. The microgel-microgel electrostatic potential is given by

$$\beta V_{mm}(r) = \begin{cases} f(r) & r < 2R_{max} \\ Z^2 L_B / r & r \geq 2R_{max} \end{cases} \quad (14)$$

$f(r)$ is the electrostatic potential that arises for overlapping configurations, assuming that the charge distribution of the particles is not affected by the mutual interpenetration. It may be calculated from numerical integration of the electric field generated by the charge distribution (see equations 1 and 2). The resulting pair interaction is a continuous and soft potential, which reaches a finite value for $r = 0$. More details of this calculation and about the shape of $f(r)$ may be found in the Appendix of Ref.[9].

Finally, we need an analytical expression for microgel-ion bare potential, $V_{mi}(r)$. The main purpose of this paper is to study the effect of the attractive/repulsive specific interactions between the polymer chains and the approaching ions. This means that, in addition to the electrostatic interaction, there are steric and specific energetic contributions that must be incorporated. Consequently, $V_{mi}(r)$ will be written as the following additive form

$$V_{mi}(r) = V_{mi}^{elec}(r) + V_{mi}^{ster-spec}(r). \quad (15)$$

The first term stands for the bare electrostatic potential between a single ion and the core-shell microgel. If the ion is located outside the microgel network ($r > R_{max}$), the electrostatic energy is given by the Coulomb interaction $Z z_i L_B / r$. However, when the ion diffuses inside the particle, the interaction potential loses the Coulombic decay, having three new different expressions corresponding to the three regions of the microgel charge distribution. Again, the details of the calculation of all these contributions may be found in Ref.[9]. The final result is the following pair potential, expressed in terms of the normalized distance $x = r/\delta$

$$\beta V_{mi}^{elec}(x) = \frac{6 Z z_i L_B}{\delta (R' + 2R'^3)} \varphi(x), \quad (16)$$

where $R' = R/\delta$, and $\varphi(x)$ is

$$\varphi(x) = \begin{cases} \frac{1}{12}(1+6R'^2) - \frac{1}{6}x^2 & x \leq R'-1 \\ \frac{(R'+1)^4 - 2R'^4}{24} + \frac{1}{60}\left[\frac{(R'-1)^5}{x} - 5(R'-1)x^3 + 5(R'(R'-2)-1)x^2 + \frac{3}{2}x^4\right] & R'-1 < x \leq R' \\ \frac{(R'+1)^4}{24} + \frac{1}{60}\left[\frac{(R'-1)^5 - 2R'^5}{x} + 5(R'+1)x^3 - 5(R'+1)^2 x^2 - \frac{3}{2}x^4\right] & R' < x \leq R'+1 \\ \frac{R'+2R'^3}{6}\frac{1}{x} & x > R'+1 \end{cases} \quad (17)$$

The second term of Eq. 15 represents the steric and specific interaction induced by the polymer network onto a single ion. It may be regarded as the interaction that the ion would feel if it was an uncharged sphere. This interaction arises when the incoming ion is placed nearby the polymer fibre, and so usually has a very short range (of the order of few solvent molecule diameters around the polymer chain). Therefore, this contribution has a non-zero value only when the ion has diffused inside the microgel volume. We will write this interaction as

$$\beta V_{mi}^{ster-spec}(r) = \begin{cases} -\ln K_i(r) & r < R_{max} \\ 0 & r \geq R_{max} \end{cases} \quad (18)$$

$K_i(r)$ are the partitioning coefficients, defined as the ratio between the ion density at distance r from the particle center and

the number density in the bulk, $K_i(r) = \rho_{mi}(r)/\rho_{0i}$ $(i = +, -)$. It should be reminded that $\rho_{mi}(r)$ corresponds here to the ionic number densities around the microgel particle neglecting the electrostatic interactions and assuming that the finite-size ionic correlations are identically zero (these correlations will be included when solving the OZ integral equations in Section 3).

$K_i(r)$ are *a priori* unknown functions. They depend on many features of the internal structure of the microgel particle, as monomer diameter, pore size distribution, polymer packing fraction, connectivity of the cross-linker monomers, and the range and strength of the short-range specific interaction between the fibres and the ion. $K_i(r)$ are also affected by the size of the ion, since large ions have less available volume when moving through the interfibre space inside the microgel. Their exact calculation involves the use of extensive and long-time consuming computer simulations. Fortunately, we can make use of the theoretical prediction for the partitioning coefficient deduced in Section 2.2. Considering that the internal structure is given by a random network of cylindrical fibres and using Eq. 10, we obtain

$$\begin{aligned} K_i(r) &= (1-e^{-\beta V_{0i}})e^{\ln(1-\phi(r))\left(1+\frac{R_i+\Delta}{R_f}\right)^2} \\ &+ e^{-\beta V_{0i}}e^{\ln(1-\phi(r))\left(1+\frac{R_i}{R_f}\right)^2} \quad i=+,- \end{aligned} \tag{19}$$

where $\phi(r)$ is the volume fraction profile of core-shell microgel, given by Eq. 1, and V_{0i} is the strength of the specific interaction between a polymer fibre and the ionic specie i.

3 Method: 3-component integral equations

Here, we employ the three-component Ornstein-Zernike (OZ) integral equations method, which has been shown to be a powerful technique to determine the ionic density profiles, the microgel net charge and the effective electrostatic interaction between a pair of microgels for this kind of mixtures[9,17]. For a multicomponent mixture of particles with spherical symmetry, they can be written as a set of six coupled integral equations that involve the convolutions of the direct correlation functions, $c_{\mu\nu}(r)$, and the radial distribution functions, $g_{\mu\nu}(r)$, defined as[30]

$$g_{\mu\nu}(r) - 1 = \frac{\rho_{\mu\nu}(r)}{\rho_{0\nu}}, \tag{20}$$

where $\rho_{\mu\nu}(r)$ is the radial density profile of specie μ around the ν-component. μ and ν are two indexes that run over the 3 species (m for microgels, $+$ for counterions and $-$ for coions). In the Fourier space, the OZ equations may be written as

$$\hat{h}_{\mu\nu}(k) = \hat{c}_{\mu\nu}(k) + \sum_{\lambda=m,+,-} \rho_{0\lambda}\hat{c}_{\mu\lambda}(k)\hat{h}_{\lambda\nu}(k), \tag{21}$$

where $h_{\mu\nu}(r) = g_{\mu\nu}(r) - 1$. The input parameters of these equations are the bulk number densities $\{\rho_{0\mu}\}$ and the six bare interactions, $\{V_{\mu\nu}(r)\}$, given by Eqs. 13–19. Moreover, since the ion-ion bare pair potentials also consider the finite size of the ions, the OZ method allows ion-ion correlations to be taken into account. This effect could be very important for deswollen states or large specific microgel-ion steric attractions, where the accumulation of ions inside or at the outer surface of the particle may give rise to significant volume effects.

In order to solve these equations, six additional closure relations connecting $h_{\mu\nu}(r)$ and $c_{\mu\nu}(r)$ with the bare interaction potentials $V_{\mu\nu}(r)$ are needed. Here, the Hypernetted Chain Closure (HNC) is used for all particle correlations, as it has shown to be a very accurate approximation for ionic microgel suspensions[9,17].

$$h_{\mu\nu}(r) = \exp\left[h_{\mu\nu}(r) - c_{\mu\nu}(r) - \beta V_{\mu\nu}(r)\right] - 1. \tag{22}$$

We are interested in the limit of very diluted suspensions ($\rho_{0m} \to 0$), where the many-body microgel-microgel interactions may be neglected. In this limit the OZ equations become separated into three sets of equations that can be solved step by step[59]. In the first step, the ion-ion distribution function are obtained, as they become uncoupled from microgel particles

$$\left.\begin{aligned} \hat{h}_{++} &= \hat{c}_{++} + \rho_{0+}\hat{c}_{++}\hat{h}_{++} + \rho_{0-}\hat{c}_{+-}\hat{h}_{+-} \\ \hat{h}_{+-} &= \hat{c}_{+-} + \rho_{0+}\hat{c}_{++}\hat{h}_{+-} + \rho_{0-}\hat{c}_{+-}\hat{h}_{--} \\ \hat{h}_{--} &= \hat{c}_{--} + \rho_{0-}\hat{c}_{+-}\hat{h}_{+-} + \rho_{0-}\hat{c}_{--}\hat{h}_{--} \end{aligned}\right\}, \tag{23}$$

where the k-dependence has been omitted. Then, the solutions are employed to calculate the microgel-ion radial distribution functions

$$\left.\begin{aligned} \hat{h}_{m+} &= \hat{c}_{m+} + \rho_{0+}\hat{c}_{m+}\hat{h}_{++} + \rho_{0-}\hat{c}_{m-}\hat{h}_{+-} \\ \hat{h}_{m-} &= \hat{c}_{m-} + \rho_{0+}\hat{c}_{m+}\hat{h}_{+-} + \rho_{0-}\hat{c}_{m-}\hat{h}_{--} \end{aligned}\right\}, \tag{24}$$

Starting from an initial guess for the direct correlation functions, $c_{\mu\nu}(r)$, equations 23 and 24 are solved iteratively using the Picard method[60] until convergence is achieved. More details about the numerical procedure may be found in Refs.[9,17]. These two steps lead to the ionic density profiles around the microgel particles, i.e. $\rho_{mi}(r) = \rho_{0i}g_{mi}(r)$.

Finally, in the third level, the already obtained microgel-ion distribution functions are employed to solve the last equation

$$\hat{h}_{mm} - \hat{c}_{mm} = \rho_{0+}\hat{c}_{m+}\hat{h}_{m+} + \rho_{0-}\hat{c}_{m-}\hat{h}_{m-}. \tag{25}$$

In the framework of the HNC approximation, the microgel-microgel effective electrostatic interaction is written as[33]

$$\beta V_{mm}^{eff}(r) = \beta V_{mm}(r) - (h_{mm}(r) - c_{mm}(r)). \tag{26}$$

It should be mentioned that the existence of other energetic contributions to the microgel-microgel interaction potential

View Article Online
DOI: 10.1039/C4SM00243A

(as steric and elastic repulsions, or the London-van der Waals attraction) do not alter the predictions achieved with this theoretical framework, provided that the microgel suspension is diluted enough to neglect many-body effects. Indeed, in the limit of infinite dilution, the ionic density profiles depend exclusively on the ion-ion and ion-microgel interactions. In addition, the calculation of $V_{mm}^{eff}(r)$ through the HNC closure (see Eq. 26) does not require the knowledge of the complete microgel-microgel-pair potential, only the electrostatic counterpart.

4 Results

In order to study the effect of the steric and specific interactions on the ionic density profiles and the microgel-microgel electrostatic effective interaction, the HNC/HNC integral equations were solved from several concentrations of 1:1 salt, ranging from extremely dilute (10^{-5}M) to highly concentrated suspensions (1M). The solvent medium is assumed to be water. The analysis covers a wide interval of the specific interaction strength, from $V_0 = -3k_BT$ to $V_0 = 3k_BT$. We study two well defined situations: in the first one coions are neutral whereas counterions are specifically attracted/repelled from the polymer fibres, and vice versa for the second one. We also need to specify the fibre and ion radius, and the range of the specific interaction. We used $R_f = 0.4$ nm, which corresponds to the average radius of the monomers of PNIPAM microgels. For the ion diameter, we could in principle employ the value in hydrated conditions. However, when an ion diffuses inside the microgel, the water layer surrounding it can be partially lost in the neighbourhood of the polymer chains[61]. For this reason, the ion radius has been chosen to be in all cases the typical one for dehydrated monovalent ions, $R_+ = R_- = 0.175$ nm. We assume that the range of the specific interaction is of the same order that the ionic radius, $\Delta = 0.175$ nm.

We also explore the effect of swelling of the microgel particles, studying the ion permeation for a totally de-swollen and swollen states. For this purpose, we borrow the experimental results of Berndt et al.[44] for PNIPAM microgels. According to these data, the shrunken configuration posses a half-width radius $R = 54$ nm, a narrow interface with $\delta = 2$ nm and a volume fraction in the particle core given by $\phi_0 = 0.52$, corresponding to a temperature $T = 50\,^{\circ}$C. The swollen state is specified by the following parameters: $R = 100$ nm, $\delta = 30$ nm, $\phi_0 = 0.078$ and $T = 25\,^{\circ}$C. The relative dielectric permittivity of the water is $\varepsilon_r = 69.9$ and 78.5, respectively. In all cases, the bare charge of the microgel particle is fixed, and given by $Z = 100$.

Before showing the results, it is interesting to illustrate the behaviour of the steric-specific contribution to the microgel-

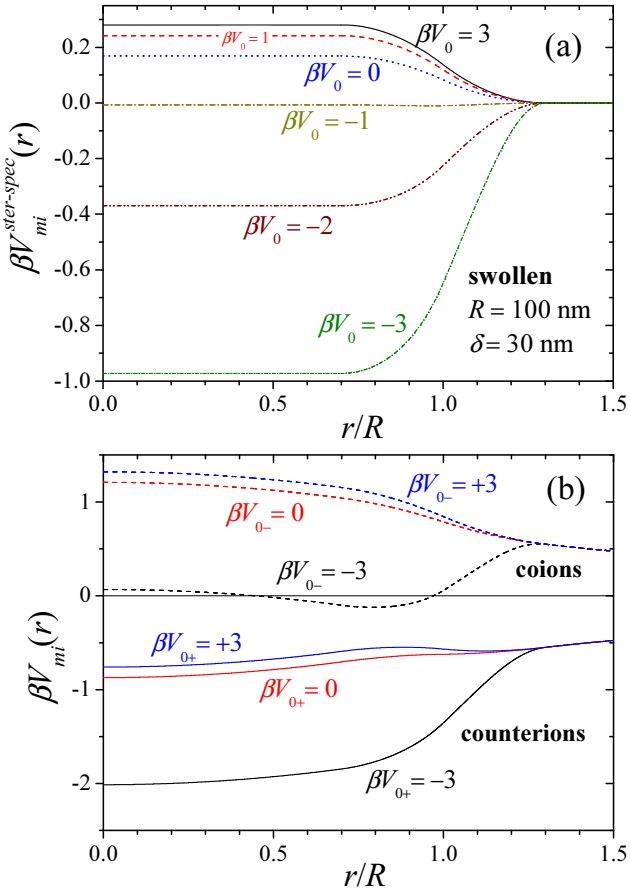

Fig. 4 (a) Steric-specific interaction bare interaction potential between and microgel particle and a single monovalent ion, $V_{mi}^{ster-spec}(r)$, calculated for different fibre-ion interaction strengths. The microgel is here in the swollen state ($R = 100$ nm, $\delta = 30$ nm). (b) Total microgel-ion bare interaction potential for counterions and coions with different fibre-ion interaction strengths. All pair potentials were obtained assuming $R_f = 0.4$ nm, $R_i = 0.175 = \Delta = 0.175$ nm and $Z = 100$.

View Article Online
DOI: 10.1039/C4SM00243A

ion interaction potential. Fig. 4(a) shows $V_{mi}^{ster-spec}(r)$ calculated from Eqs. 18 and 19 considering the swollen state, for different strengths of the specific fibre-ion interaction, and for the set of parameters fixed above. For the swollen state, this interaction is a smooth and monotonous function of the distance to the particle center, repulsive for $\beta V_0 > -0.973$ and attractive for $\beta V_0 < -0.973$ (for $\beta V_0 = -0.973$ the steric and specific interactions compensate one to each other so $V_{mi}^{ster-spec} \approx 0$). This result is consistent with the fact that the partitioning coefficient always increases with the volume fraction for $\phi \in [0, 0.078]$ (see the left vertical line in Fig. 2). Fig. 4(b) plots the total microgel-ion bare interaction, which includes both the electrostatic and the steric-specific contributions. For counterions, the steric-specific interaction calculated for $\beta V_{0+} = -3$ leads to an emphasized attractive well that is gradually reduced as the steric-specific attraction decreases and becomes repulsive. In this case, the polymer volume fraction is so small that the steric-specific repulsion is not enough to compensate the electrostatic attraction. However, it should be kept in mind that this behaviour can be very different for weakly charged microgel particles, where the steric repulsion could overcome the electrostatic term, yielding a repulsive interaction even for counterions. Analogously, for coions, the steric-specific attraction for $\beta V_{0-} = -3$ also causes the formation of an attractive well, but in this case there is also an electrostatic repulsive barrier of about $0.55 k_B T$ that partially prevents the coion permeation. For $\beta V_{0-} > -0.973$ the electrostatic repulsion with the microgel is favoured by the steric-specific term.

Fig. 5(a) depicts again $V_{mi}^{ster-spec}(r)$, but now for a de-swollen microgel. In this case, for $\beta V_0 > 0$ we obtain again a monotonic repulsion, with the difference that the barrier is now sharper and stronger caused by the larger polymer volume fraction ($\phi_0 = 0.52$). It can be shown that the specific attraction dominates over the steric repulsion in the particle core for $\beta V_0 < -1.86$. However, a new effect comes up when $\beta V_0 < 0$. Indeed, the volume fraction in the particle core is so high that the competition between the specific attraction and the steric repulsion gives rise a maximum of the partitioning coefficient with ϕ (see again Fig. 2). Thus, the steric-specific interaction potential also shows a narrow attractive well located at the external shell of the particle. This means that the solute is more likely to be accumulated in the shell of the collapsed microgel than in the particle core. The total microgel-ion interaction (see Fig. 5(b)) shows significant differences from the swollen state. Indeed, the attraction for counterions with $\beta V_{0+} < -1.86$ is now more pronounced and shows the additional attractive well located in the particle shell. Surprisingly, this attraction becomes an important repulsive barrier as we reach positive values of βV_{0+}, hindering the counterions diffusion inside the microgel particle. For coions and $\beta V_{0-} < -1.86$ we obtain again an attractive well bounded by

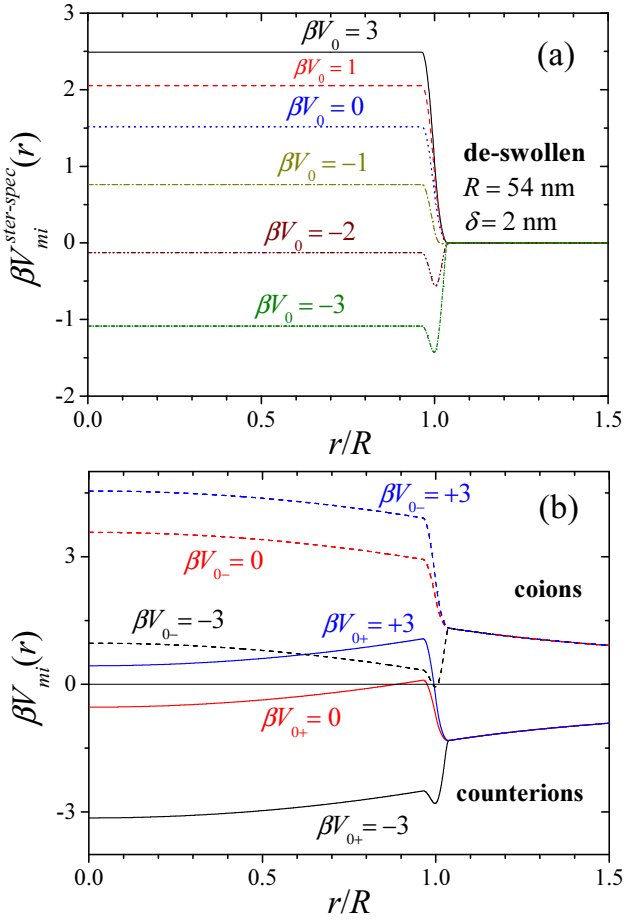

Fig. 5 Same as Fig. 4 but for the de-swollen configuration ($R = 54$ nm, $\delta = 2$ nm).

View Article Online
DOI: 10.1039/C4SM00243A

a electrostatic repulsive barrier of $1.33k_BT$. In contrast, for $\beta V_{0-} > -1.86$ the steric-specific effect is repulsive and induces a very sharp and large repulsive barrier of several k_BT, resembling the situation for hard colloids.

4.1 Ionic density profiles

We first show the ionic density profiles around and inside the porous microgel particle for the swollen configuration ($R = 100$ nm and $\delta = 30$ nm). In this case, the polymer packing fraction smoothly increases along the extended shell. Fig. 6(a) illustrates the radial distribution functions for counterions and coions, respectively, calculated for an electrolyte concentration $[\cdot] = 10^{-3}$M. In addition to the electric and steric interactions with the microgel, we consider that counterions interact specifically with the polymer fibres ($V_{0+} \neq 0$), while coions are inert ($V_{0-} = 0$). For attractive specific interactions, counterions (lines with symbols) emigrate to the interior of the microgel due to the superposition of the electrostatic and specific attractions. Here, we encounter the unusual behaviour that coions (dashed lines) are also adsorbed inside the microgel even though they are electrostatically and sterically repelled. This effect is caused by the electrostatic attraction induced by the excess counterion cloud inside the particle, which is able to invert the net charge of the particle, as we will see later on.

By reducing the specific attraction the counterion penetration decreases. For $\beta V_{0+} = -1$ the steric and specific interactions almost cancel each other, and the electrostatic attraction becomes the the dominant contribution. However, we observe that the counterions are depleted from the internal region of the microgel regardless the electrostatic attraction. Again, the explanation of the phenomenon relies on the ion correlations. Indeed, since coions feel an additional steric repulsion, they are more efficiently depleted from the internal volume of the particle, pulling electrostatically the counterions outside. This effect is emphasized by increasing V_{0+} to larger positive values, and so favouring the depletion of counter- and coions inside.

Fig. 6(b) shows the same results than before, but assuming that coions are the ones that interact specifically with the polymer fibres. For $\beta V_{0-} < -0.973$ the microgel-coion interaction shows an attractive well. Hence, coions are also attracted inside the microgel, regardless the electrostatic repulsion. For repulsive steric-specific interactions, coions are depleted from the internal region. Then, the electrostatic attraction between the coion cloud outside and the internal counterions provokes again a decrease of the counterion concentration inside the particle.

Representative results for the ionic density profiles around a de-swollen microgel are shown in Fig. 7(a) calculated again for $[\cdot] = 10^{-3}$M, and assuming that the counterions inter-

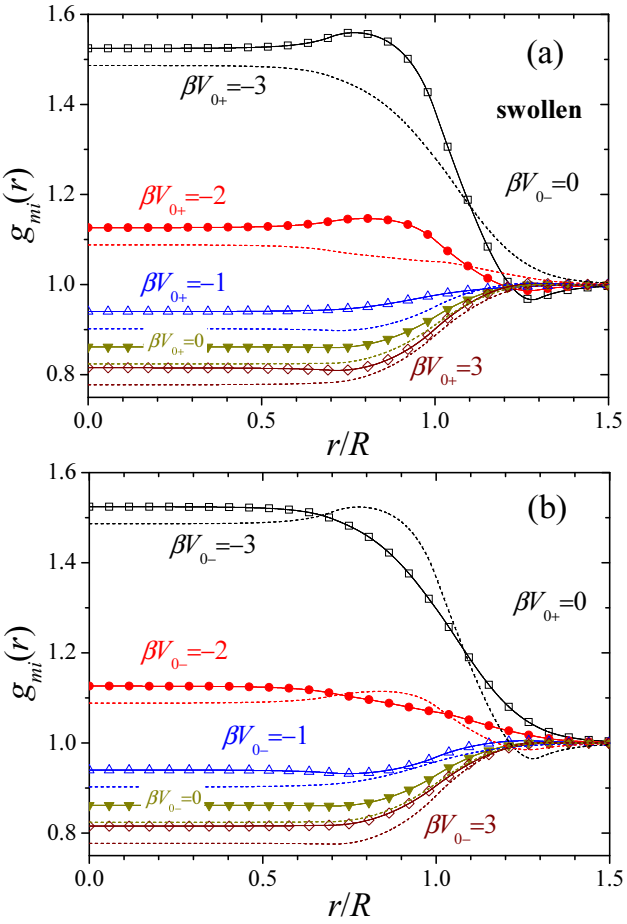

Fig. 6 Radial distribution function of the monovalent ions inside and around the microgel particle in the swollen configuration ($R = 100$ nm and $\delta = 30$ nm), for several fibre-ion specific interaction strength ranging from $V_0 = -3k_BT$ to $V_0 = +3k_BT$. Plot (a) shows the counterions and coion density profiles (symbols and dashed lines, respectively), being the counterions the ones that interact specifically with the polymer fibre, whereas coions are inert. Plot (b) depicts the same curves, but now with inert counterions and coions interacting specifically. In all cases, the salt concentration is $[\cdot] = 10^{-3}$M and the bare charge of the microgel particle is $Z = 100$.

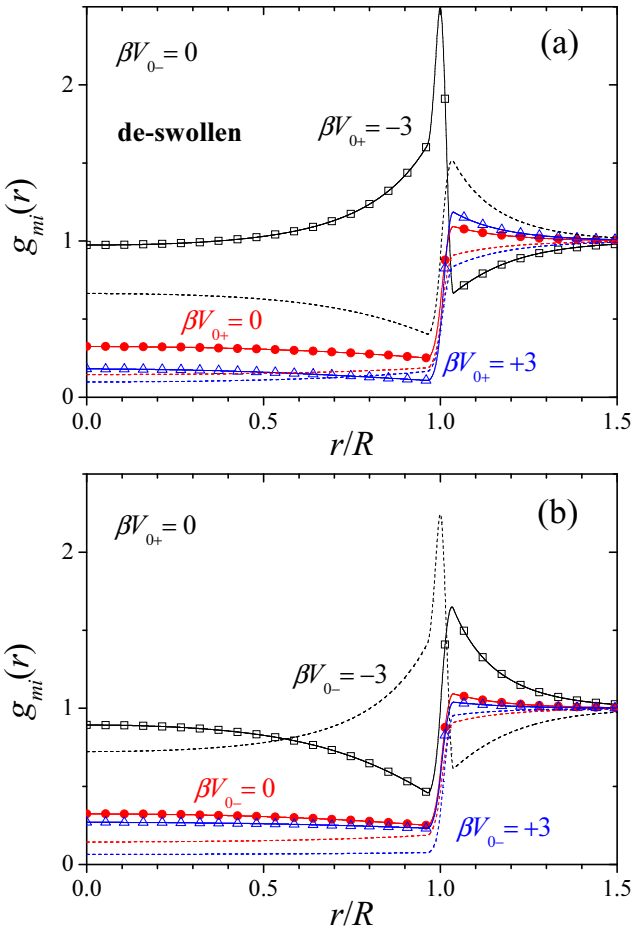

Fig. 7 Same as Fig. 6 but for the de-swollen configuration ($R = 54$ nm and $\delta = 2$ nm).

act specifically with the polymer fibres. For $\beta V_{0-} = -3$ the counterion density profile (line with symbols) shows a thin and very large adsorption peak located in the shell of the particle. This means that the counterion penetration inside the polymer matrix in the shrunken state is not so large as could be expected. On the contrary, counterions are more likely to be accumulated in the particle shell instead of in the core, in spite of the electrostatic attraction. In fact, this maximum is a straightforward consequence of the narrow potential well induced by the specific attraction in the microgel-counterion interaction (see Fig. 5(b)). Under a more intuitive point of view, the adsorption of counterions in the shell is connected to the increase of the steric repulsion in the particle core due to the larger polymer packing fraction here, that partially compensates the specific attraction.

The coion density profile (dashed line) also shows a peak in the external shell of the de-swollen microgel. This less important peak is mainly originated by the steric repulsive barrier that inert coions feel when they try to diffuse inside the microgel core. The repulsive barrier is higher that for the swollen configuration, giving rise to a significant depletion of coions in the particle core. For repulsive specific interactions $\beta V_{0+} > 0$ the potential well completely disappears and it is replaced by a rather significant repulsive barrier that prevents the counterions from entering inside the microgel. This may be clearly observed in Fig. 7(a), where $g_{m+}(r)$ shows a internal depletion region and a external maximum induced by this repulsive barrier.

Fig. 7(b) depicts again the ionic density profiles in the shrunken configuration, but taking the coions as the ones that interact specifically. Again, for a strongly attractive specific interaction ($\beta V_{0-} = -3$) the coion density profile has a maximum placed in the particle shell. This maximum is also caused by the narrow attractive well of $V_{m-}(r)$. However, the height of the peak is smaller than the one observed for counterions, which is accompanied by a more efficient depletion in the particle core due to the fact that the electrostatic term is now repulsive instead of attractive. Analogously, the counterion-microgel steric repulsive barrier inhibits the counterion permeation and encourages the formation of a repulsive peak, also in the particle shell. For $\beta V_{0-} > 0$ we observe an enhanced depletion of coion, as expected. Analogously, counterions are also pulled outside by the external coions, causing an additional decrease of the counterion concentration in the particle core.

4.2 Microgel net charge: charge inversion and overcharging

The net charge of the microgel is defined as the total charge contained inside the particle, including the charged monomers, conterions and coions. Z_{net} represents the *real*

View Article Online
DOI: 10.1039/C4SM00243A

charge that any incoming ion or charged colloid will feel when approaching to the microgel particle. Z_{net} is a very important magnitude since it is involved, for instance, in the stability of the suspension. It may be easily calculated from integration of the internal ionic density profiles

$$Z_{net} = Z - 4\pi \int_0^{R_{max}} (\rho_{m+}(r) - \rho_{m-}(r))\, r^2 dr. \qquad (27)$$

Fig. 8 plots the Z_{net}/Z obtained in the swollen configuration for different specific interactions, as a function of the screening constant, κR (κ is the inverse Debye length, defined as $\kappa = (4\pi L_B \sum_i \rho_{0i} z_i^2)^{1/2} = (8000\pi L_B N_a [\,\cdot\,])^{1/2}$, where N_a is the Avogadro's number). We better use κR instead the salt concentration because in this way the theoretical results can be easily transfered to particles with other size. Fig. 8(a) shows $Z_{net}/|Z|$ considering that only counterions interact specifically with the polymer fibres. For attractive specific interactions ($V_{0+} < 0$) there is a critical salt concentration (to which we will refer as the inversion point) that totally neutralizes the particle bare charge. The inversion point shifts to larger salt concentrations as the specific attraction decreases, since then we need a larger counterion bulk concentration to induce the migration of enough counterions inside the microgel to compensate the bare charge. For salt concentrations above the inversion point, the inverted net charge keeps growing, inducing the overcharging of the microgel. It is important to emphasize that the charge inversion observed here is caused exclusively by the specific attraction with the microgel, and does not have any relation with the overcharging effect induced by multivalent ions due to electrostatic ion correlations. In fact, charge reversal never occurs if we exclusively include ion-microgel electrostatic interactions (see bold solid line in Fig. 8(a)).

The particle overcharging does not grow indefinitely as a function of the salt concentration. On the contrary, it reaches a maximum and then decreases again for large enough $[\,\cdot\,]$. A similar behaviour has been also experimentally observed in suspensions of hard charged particles[62], where the addition of monovalent salt to an already charged-inverted colloidal suspension (by means of trivalent counterions) induces a decrease of the electrophoretic mobility, which is strongly connected to the net charge of the particle. In both cases, the explanation of this effect fall in the strong screening that arises at high electrolyte concentrations. Moreover, diverse theories of charge inversion and Monte Carlo simulations predict also that the phenomenon of overcharging weakens and even tends to disappear in the presence of large amounts of monovalent electrolyte[63,64]

For repulsive counterion-microgel specific interactions ($V_{0+} \geq 0$) charge inversion does not occur, and Z_{net} smoothly tends to zero as the electrolyte concentration increases. This result is expected, since under this situation counterions are less likely to diffuse inside the microgel. The increase of V_{0+}

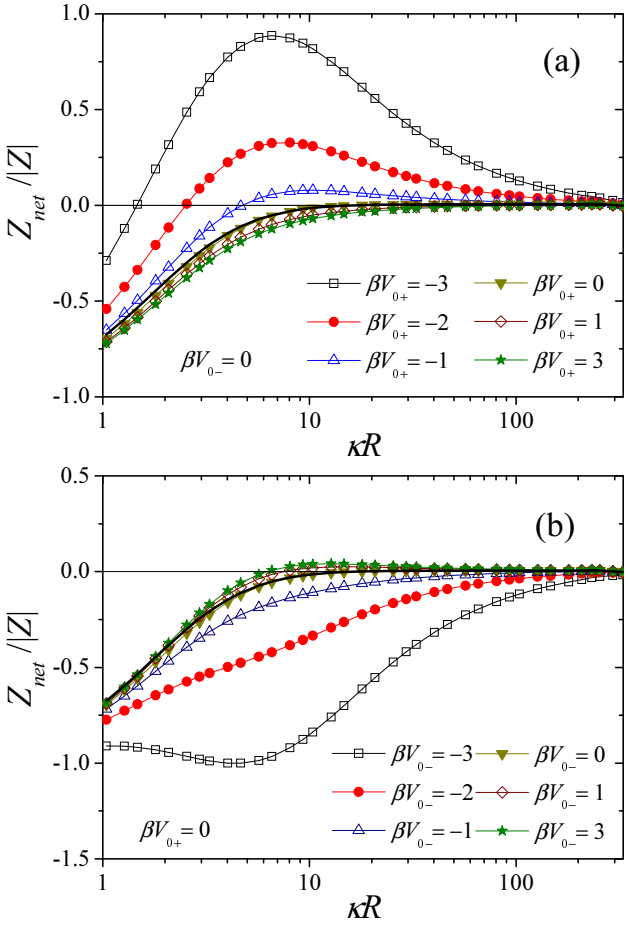

Fig. 8 Net charge of the microgel particle normalized by the bare charge ($Z_{net}/|Z|$) as a function of the screening constant, κR, calculated for the swollen state ($R = 100$ nm and $\delta = 30$ nm). In plot (a) counterions interact specifically with the polymer fibre whereas coions are inert (vice versa in plot (b)). In both cases $Z = 100$. Bold solid line is obtained assuming a perfectly permeable microgel that does not interact sterically neither specifically with the ions.

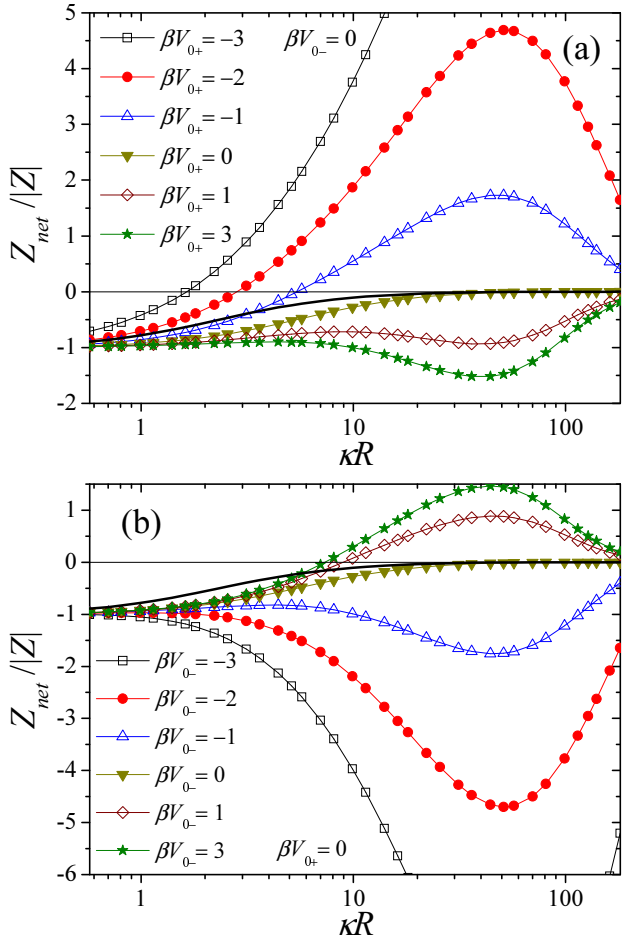

Fig. 9 Same as Fig. 8 but for the de-swollen state ($R = 54$ nm and $\delta = 2$ nm). Notice that the charge inversion and overcharging effects are now emphasized.

favours the counterion exclusion in the particle core, thereby making the charge screening less efficient. This is translated into an enhancement of $|Z_{net}|$. However, this effect is quite small, since the steric-specific repulsion for the swollen state only represents a minor correction even for $\beta V_{0+} = 3$, as may be observed in Fig. 4(b).

In Fig. 8(b) we plot the same sort of results, but assuming that the coion interact specifically with the polymer matrix, while counterions are inert. For strong microgel-coion attractions (see for instance the curve for $\beta V_{0-} = -3$) the additional adsorption of coions driven by the specific attraction is able to overcome the electrostatic repulsion. As a result of this, the net charge of the microgel grows with the salt concentration, giving rise to a phenomenon which has been called *true overcharging*[65]. Again, the increase of $|Z_{net}|$ reaches a maximum value at a salt concentration corresponding to $\kappa R \approx 4.5$. For salt concentrations above this one, the charge screening effect brings the net charge to zero. For smaller coion-microgel specific attractions there is no evidence of any maximum, and $|Z_{net}|$ decays monotically to zero. However, for $\beta V_{0-} < -0.97$ the values of $|Z_{net}|$ are always larger than the ones predicted for perfectly permeable microgel in the absence of steric-specific interactions. Finally, it is interesting to note that for strong coion-microgel specific repulsions (see the curve for $\beta V_{0-} = 3$) a small charge inversion of the microgel is also observed, induced by the coion exclusion.

The situation changes significantly when studying the de-swollen state. Then, the increase of the internal polymer packing fraction causes a great enhancement or suppression of the ion penetration, depending on whether steric-specific interactions are attractive or repulsive, respectively. Fig. 9(a) shows the results for counterions with specificity. On the one hand, the charge inversion predicted with attractive conterion-microgel specific interactions is now huge, leading to an enhanced particle overcharging phenomenon. This accumulation of counterions occurs in the particle shell, as it has been shown before. For large salt concentration the charge screening finally induces a decrease of Z_{net}. However, the salt concentration necessary to achieve this regime is much larger than for the swollen configuration, since it is required a large amount of ions to compensate the effect of the specific attraction. On the other hand, for large repulsive counterion-microgel specific interactions (see the curve for $\beta V_{0+} = 3$), counterions are so strongly expelled from the particle core (compared to coions) that $|Z_{net}|$ can even increase for large enough electrolyte concentration.

Finally, the net charge of the microgel for the case of specific coions and inert counterions is shown in Fig. 9(b). Again, an enhancement of the net charge is observed for attractive specific coion-microgel interactions. The accumulation of coions in the shell is here so important that an enormous true overcharging of the particle emerges. For repulsive interac-

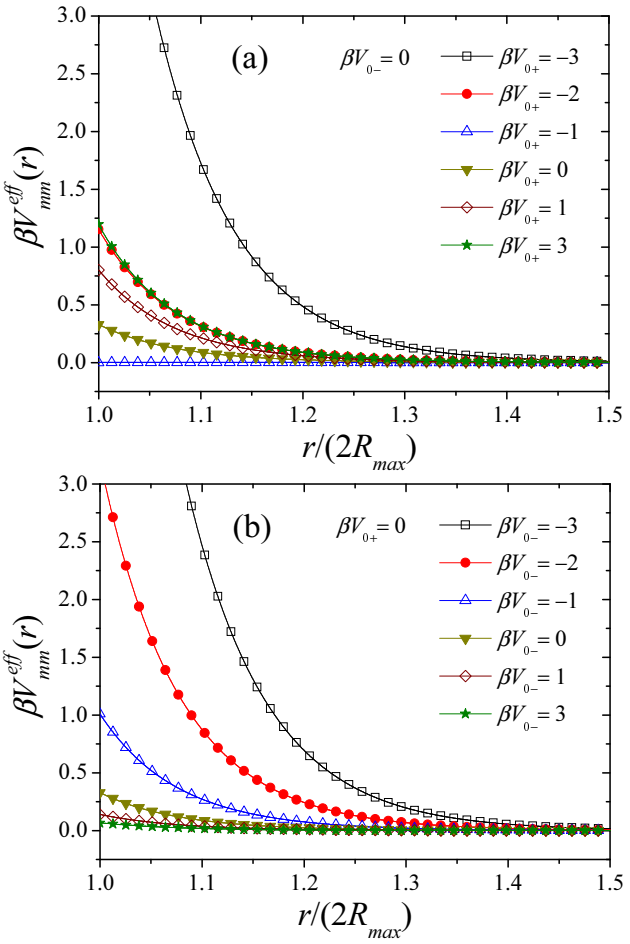

Fig. 10 Effective interaction potentials between a pair of microgel particles for diferent polymer-ion specific interaction strengths. In plot (a) counterions interact specifically with the polymer fibre whereas coions are inert (vice versa in plot (b)). In both cases the microgel particles are in the de-swollen state, $Z = 100$ and $[\cdot] = 10^{-3}$M.

tions ($V_{0-} > 0$), coions are efficiently excluded at the time that counterions are able to penetrate more easily. As a result of this, a charge inversion is found. However, in this case the overcharging is emphasized by the fact that the specific repulsive barrier for the de-swollen configuration is larger than the one for the swollen state.

4.3 Effective pair interaction between microgel particles

The specific interaction between the microgel particle and the surrounding ions has also important implications on the effective potential between pairs of microgel particles, and so on the stability of the suspension. To illustrate this, we show in Fig. 10 the microgel-microgel effective interaction obtained from Eq. 26. It is important to note that this pair interaction has an electrostatic nature, since it only includes the effect of the direct electrostatic interaction plus the interaction induced by the ionic clouds inside and around the microgel particles. However, there are additional steric and elastic energetic terms that emerge when the two cross-linked polymer chains become deformed after overlapping[12,34,66]. Since those other contributions are not considered in this work, we only plot $V_{mm}^{eff}(r)$ for non-overlapping distances, $r > 2R_{max}$.

Fig. 10(a) shows $V_{mm}^{eff}(r)$ calculated for a salt concentration given by $[\cdot] = 10^{-3}$M, assuming that counterions interact specifically with the microgel. The figure includes data for attractive and repulsive specific interactions. In all cases, the effective interaction decays with the interparticle distance following a Yukawa dependence

$$V_{mm}^{eff}(r) = \frac{Z_{eff}^2 L_B}{(1+\kappa R_{max})^2}\frac{e^{-\kappa(r-2R_{max})}}{r}, \qquad (28)$$

where Z_{eff} is the effective charge of the microgel, which is a renormalized charge strongly connected to Z_{net}. This functional form for the electrostatic effective interaction has been found to hold in salty suspensions of ionic nanogel suspensions for both uniformly charged and core-shell ionic nanogel suspensions in the swollen or de-swollen states[9,10,17].

As we increase βV_{0+} from -3 to 3 the effective interaction shows a reentrant behaviour. Indeed, for $\beta V_{0+} = -3$ the microgel particle has already inverted its charge, and $Z_{net} \approx 2.16|Z|$. The effective interaction is thereby repulsive. Both the net charge and the interparticle repulsion strength progressively decrease as the specific attraction is reduced. For $\beta V_{0+} = -1$ the system reaches the inversion point for this salt concentration, where $Z_{net} = 0$. Under this particular condition, the electrostatic effective pair potential is practically zero and the microgel-microgel interaction is controlled by the London-van der Waals attraction, which has been proved to be very important between de-swollen microgels[1,67]. In other words, the microgel suspension becomes unstable and formation of clusters is expected. Upon increasing βV_{0+} to greater specific repulsions, the absolute value of Z_{net} increases again, giving rise to a re-stabilization of the suspension. This may be clearly seen in Fig. 10(a), where the strength of the Yukawa barrier grows with the specific repulsion.

Fig. 10(b) plots $V_{mm}^{eff}(r)$ under identical conditions, but considering that coions are the ones which interact specifically with the microgel. In this case, the reentrant behaviour is not achieved due to the absence of charge inversion. As it may be observed, the strength of the Yukawa repulsive barrier simply decreases as we shift the specific interaction from attraction (where the particle is truly overcharged due to the specific adsorption of coions) to repulsion.

5 Conclusions

The effects that the electrostatic, steric and short-range specific interactions (hydrophobic, hydrophilic, hydrogen bonds,...) have on the permeation of ions inside a porous cross-linked microgel particle has been studied by solving the three-component Ornstein-Zernike integral equations within the HNC approximation. For this purpose, a theory based on the partitioning coefficient has been used to coarse-grain the internal degrees of freedom of the polymer network. The results clearly indicate that the ion penetration is the consequence of a complex interplay between all these interactions. Moreover, the degree of swelling of the particle also plays an important role, as it strongly enhances the steric and specific interactions as the microgel shrinks.

Our results predict that for a fixed bare charge density (given by Eq. 2), the inclusion of a short-range specific attraction between counterions and the cross-linked polymer fibres of the microgel causes an enhanced counterion adsorption that is able to invert the microgel net charge. The inversion point shifts to smaller salt concentration as the specific attraction increases. For the case of coions, the specific attraction is also able to induce the coion adsorption even though they are electrostatic repelled. In addition, this effect enhances the microgel charge (true overcharging). The interplay between steric repulsion and specific adsorption leads to a counterion adsorption that mainly occurs in the particle core for swollen states and in the shell for de-swollen morphologies. These results are consistent with experimental observations, where it is clearly shown that the uptake of water-solute drugs (or ions) inside microgel particle becomes strongly enhanced by the hydrophobic character of the drug molecules[21,68]. For repulsive ion-fibre specific interactions, our theoretical predictions indicate that ions become depleted from the internal core and become accumulated in the external shell. This effect is more important for shrunken microgels, where the steric-specific repulsive barrier is so large that can even overcome the electrostatic interaction. Thus, a depletion region is formed inside the particle which also favours the particle overcharging for repelled coions and the true overcharging for repelled counterions.

Finally, the electrostatic effective microgel-microgel pair potential is in all cases a repulsive interaction. However, the strength of the repulsion vanishes as the electrolyte concentration approaches the inversion point, leading to a reentrant stability of the microgel suspension.

It is important to point out some limitations of our theory. First of all, the model assumes that the polymer chains inside the nanogel are rigid. However, it is well known that the polymer fibres between two cross-linker monomers are flexible and can be locally extended, compressed and deformed when an incoming electrolyte diffuses inside the particle. This means that, in principle, ion permeability can be larger than the one predicted using the steric-specific interaction provided by Eqs. 18 and 19. We are now working in this direction, comparing the theoretical predictions with results obtained with coarse-grained computer simulations[36]. Furthermore, a Another important factor affecting the penetration of a charged solute is the cross-linker density and the distribution of functional groups in the microgel. Experimental results performed with PNIPAM show that a uniform distribution of charged groups inside the particle is able to bind more drug than surface-localized microgels, whereas a distribution of bare charged groups in the shell of the particle emphasizes the condensation of drug on the microgel surface that hinders the diffusion of additional drug[69]. Finally, it would be desirable to implement these inherent steric and specific interactions into a more general theory able to incorporate the swelling and shrinking of the microgel particle induced by the presence of electrolyte, in such a way that the ionic density profiles and the equilibrium swelling ratio are consistently determined. In order to correctly account for this particle swelling, the elastic free-energy of the cross-linked polymer network should be necessarily included, somewhat like the model recently proposed by Yigit *et al*[13] or Sing *et al.*[14]. Nevertheless, in spite of its simplicity, the present model can always be applied to interpret the experimental results, provided that the equilibrium swelling state is already known and used as an input parameter in our calculations. Therefore, the analysis presented here may serve as a starting point for a more complete study in future work, where comparisons to experiments should also be performed.

Acknowledgements

The Spanish Ministerio de Economía y Competitividad (project MAT2012-36270-C04-02) is gratefully acknowledged for financial support. The authors also thanks Dr. Alberto Martín-Molina and Dr. Delfi Bastos-González for helpful discussions.

References

1 A. Fernández-Nieves, H. M. Wyss, J. Mattsson, and D. A. Weitz, *Microgel Suspensions: Fundamentals and Applications* (Wiley-VCH, Weinheim, 2011).
2 M. J. Murray and M. Snowden *Adv. Colloid Interface Sci.*, 1995, **54**, 73–91.
3 B. R. Saunders and B. Vincent, *Adv. Colloid Interface Sci.*, 1999, **80**, 1–25.
4 B. R. Saunders, N. Laajam, E. Daly, S. Teow, X. Hu and R. Stepto, *Adv. Colloid Interface Sci.*, 2009, **147-148**, 251–262.
5 J. Ramos, A. Imaz, J. Callejas-Fernández, L. Barbosa-Barros, J. Estelrich, M. Quesada-Pérez and J. Forcada, *Soft Matter*, 2011, **7**, 5067–5082.
6 A. Imaz and J. Forcada, *J. Polym. Sci., Part A: Polym. Chem.*, 2010, **48**, 1173–1181.
7 J. Ramos, A. Imaz and J. Forcada, *Polym. Chem.*, 2012, **3**, 852–856.

8 S. V. Vinogradov, *Nanomedicine*, 2010, **5**, 165–168.
9 A. Moncho-Jordá, J. A. Anta and J. Callejas-Fernández, *J. Chem. Phys.*, 162 10 *Journal Name*, 2010, **[vol]**, 1–16
10 A. R. Denton, *Phys. Rev. E*, 2003, **67**, 011804. Erratum *ibid*, 2003, **68** 049904.
11 D. Gottwald, C. N. Likos, G. Kahl and H. Löwen, *Phys. Rev. Lett.*, 2004, **92**, 068301.
12 J. Riest, P. Mohanty, P. Schurtenberger and C. N. Likos, *Z. Phys. Chem.*, 2012, **226**, 711–735.
13 C. Yigit, N. Welsch, M. Ballauff and J. Dzubiella, *Langmuir*, 2012, **28**, 14373–14385.
14 C. E. Sing, J. W. Zwanikken and M. Olvera de la Cruz, *Macromolecules*, 2013, **46**, 5053–5065.
15 E. M. Johnson and W. M. Deen, *J. Colloid Interface Sci.*, 1996, **178**, 749–756.
16 M. J. Lazzara, D. Blankschtein and W. M. Deen, *J. Colloid Interface Sci.*, 2000, **226**, 112–122.
17 A. Moncho-Jordá, *J. Chem. Phys.*, 2013, **139**, 064906.
18 W. Kunz, P. Lo Nostro and B. W. Ninham, *Curr. Opin. Colloid Interface Sci.*, 2004, **9**, 1–18.
19 J. Faraudo and A. Martín-Molina, *Curr. Opin. Colloid Interface Sci.*, 2013, **18**, 517–523.
20 A. Martín-Molina, C. Calero, J. Faraudo, M. Quesada-Pérez, A. Travesset and R. Hidalgo-Alvarez, *Soft Matter*, 2009, **5**, 1350–1353.
21 T. López-León, A. Alaïssari, J. L. Ortega-Vinuesa and D. Bastos-González, *ChemPhysChem*, 2007, **8**, 148–156.
22 F. Hofmeister, *Arch. Exp. Pathol. Phamakol*, 1888, **24**, 247–260.
23 K. D. Collins and M. W. Washabaugh, *Q. Rev. Biophys.*, 1985, **18**, 323–422.
24 R. Leberman and K. D. Soper, *Nature*, 1995, **378**, 364–366.
25 K. D. Collins, *Methods*, 2004, **34**, 300–311.
26 J. Chick, S. Mizzarhi, S. Chi, V. A. Parsegian and D. C. Rau, *J. Phys. Chem. B*, 2005, **109**, 9111–9118.
27 E. Daly and B. R. Saunders, *Langmuir*, 2000, **16**, 5546–5552.
28 L. Zha, J. Hu, C. Wang, S. Fu and M. Luo, *Colloid Polym. Sci.*, 2002, **280**, 1116–1121.
29 F. Jiménez-Angeles and M. Lozada-Cassou *J. Phys. Chem. B*, 2004, **108**, 7286–7296.
30 J. P. Hansen and I. R. McDonald, *Theory of Simple Liquids* 3rd Ed. (Academic Press, USA, 2006).
31 C. Caccamo, *Phys. Rep.*, 1996, **274**, 1–105.
32 A.A. Louis, *Phylos. Trans. R. Soc. London A*, 2001, **359**, 901.
33 S. Karanikas, J. Dzubiella, A. Moncho-Jordá and A. A. Louis, *J. Chem. Phys.*, 2008, **128**, 204704.
34 D. Gottwald, C. N. Likos, G. Kahl, and H. Löwen, *J. Chem. Phys.*, 2005, **122**, 074903.
35 M. Quesada-Pérez, J. A. Maroto-Centeno and A. Martín-Molina, *Macromolecules*, 2012, **45**, 8872–8879.
36 M. Quesada-Pérez and A. Martín-Molina, *Soft Matter*, 2013, **9**, 7086–7094.
37 J. A. Anta, and S. Lago, *J. Chem. Phys.*, 2002, **116**, 10514.
38 J. A. Anta, *J. Phys.: Condens. Matter*, 2005, **17**, 7935–7953.
39 M. Stieger, W. Richtering, J. S. Pedersen and P. Lindner, *J. Chem. Phys.*, 2004, **120**, 6197–6206.
40 X. Wu, R. H. Pelto This journal is © The Royal Society of Chemistry [year] *loid Polym. Sci.*, 1994, **272**, 467–477.
41 A. Fernández-Barbero, A. Fernández-Nieves. I. Grillo and E. López-Cabarcos, *Phys. Rev. E*, 2002, **66**, 051803.
42 S. Meyer and W. Richtering, *Macromolecules*, 2005, **38**, 1517–1519.
43 I. Berndt, J. S. Pedersen, P. Lindner and W. Richtering, *Langmuir*, 2006, **22**, 459–468.
44 I. Berndt, J. S. Pedersen and W. Richtering, *J. Am. Chem. Soc.*, 2005, **127**, 9372–9373.
45 A. Fernández-Nieves, A. Fernández-Barbero, F. J. de las Nieves and B. Vincent, *J. Phys.: Condens. Matter*, 2000, **12**, 3605–3614.
46 G. Romeo, L. Imperiali, J.-W. Kim, A. Fernández-Nieves and D. A. Weitz, *J. Chem. Phys.*, 2012, **136**, 124905.
47 J. L. Anderson and J. A. Quinn, *Biophys. J.*, 1974, **14**, 130–150.
48 R. Langer and J. Folkman, *Nature (London)*, 1976, **263**, 797–800.
49 J. C. Giddings, E. Kucera, C. P. Russell and M. N. Myers, *J. Phys. Chem.*, 1968, **72**, 4397–4408.
50 L. A. Fanti and E. D. Glandt, *J. Colloid Interface Sci.*, 1990, **135**, 385–395.
51 L. A. Fanti and E. D. Glandt, *J. Colloid Interface Sci.*, 1990, **135**, 396–404.
52 F. G. Smith and W. M. Deen, *J. Colloid Interface Sci.*, 1983, **91**, 571–590.
53 A. G. Ogston, *Trans. Faraday Soc.*, 1958, **54**, 1754–1757.
54 E. M. Johnson, D. A. Berk, R. K. Jain and W. M. Deen, *Biophys J.*, 1995, **68**, 1561–1568.
55 J. N. Israelachvili, *Intermolecular and Surface Forces* 3rd Ed. (Academic Press, USA, 2011).
56 J. Wu, B. Zhou and H. Hu, *Phys. Rev. Lett.*, 2003, **90**, 048304.
57 H. Senff and W. Richtering, *J. Chem. Phys.*, 1999, **111**, 1705–1711.
58 D. A. Sessoms, I. Bischofberger, L. Cipelletti and V. Trappe, *Phil. Trans. R. Soc. A*, 2009, **367**, 5013–5032.
59 G. I. Guerrero-García, E. González-Tovar, M. Lozada-Casou and J. Guevara-Rodríguez, *J. Chem. Phys.*, 2005, **123**, 034703.
60 N. H. Shah, *Numerical Methods with C++ programming* (PHI, 2009).
61 Y. Zhang, S. Furyk, L. B. Sagle, Y. Cho, D. E. Bergbreiter and P. S. Cremer, *J. Phys. Chem.*, 2007, **111**, 8916–8924.
62 A. Martín-Molina, M. Quesada-Pérez, F. Galisteo-González and R. Hidalgo-Alvarez, *J. Phys.: Condens. Matter*, 2003, **15**, S3475–S3483.
63 A. Martín-Molina, M. Quesada-Pérez and R. Hidalgo-Alvarez, *J. Phys. Chem. B*, 2006, **110**, 1326–1331.
64 A. Martín-Molina, J. A. Maroto-Centeno, R. Hidalgo-Alvarez and M. Quesada-Pérez, *J. Chem. Phys.*, 2006, **125**, 144906.
65 M. Lozada-Cassou and F. Jiménez-Angeles, arXiv:physics/0105043v2.
66 J. L. Johnson, *Normal contact of elastic solids - Hertz theory* (Cambridge University Press, 1985).
67 H. M. Crowther and B. Vincent, *Colloid Polym. Sci.*, 1998, **276**, 46–51.
68 T. Hoare and R. Pelton, *Langmuir*, 2008, **24**, 1005–1012.
69 R. Yoshida, K. Sakai, T. Ukano, Y. Sakurai, Y. H. Bae and S. W. Kim, *J. Biomater. Sci. Polym. Ed.*, 1991, **3**, 155–162.